HEAT TRANSFER ENGINEERING
2022, VOL. 43, NO. 11, 922–936
https://doi.org/10.1080/01457632.2021.1919972

Investigation of the Parameter-Dependence of Topology-Optimized Heat Sinks in Natural Convection

Han-Ling Li[a], Dai-Yan Lan[b], Xian-Ming Zhang[b], and Bing-Yang Cao[a]

[a]Key Laboratory for Thermal Science and Power Engineering of Ministry of Education, Department of Engineering Mechanics, Tsinghua University, Beijing, China; [b]Thermal Design Reliability Department, ZTE Corporation, Shenzhen, China

ABSTRACT

The thermal design of natural convection heat sinks is critical to the heat management of electronic devices. In this paper, topology optimization (TO) with a new parameter advancing scheme is employed to study the effect of the heating power, heat source size, allowed volume and material thermal conductivity on the optimized design of natural convection heat sinks. Except for the heating power, the other three factors also play an important role on the optimization results. For the small heating power, TO predicts the tree-like heat sink with many secondary-branches to improve heat conduction, but the specific structure is highly dependent on the heat source size, allowed volume and material thermal conductivity. For the large heating power, TO prefers to produce the taper-like heat sink where the tiny branches fade away to adapt to the strong flow, and the influences of the other three factors are reduced. However, two primary branches that connect the heat source and top corners of the design domain always exist, indicating that they are the most effective ways to improve heat transfer. This work has highlighted the impact of different parameters in TO of natural convection heat sinks and provides a more in-depth understanding of the design guidelines.

Introduction

Modern wireless communication has entered the age of the 5th generation (5 G), which has the advantages of high data transfer rate, high capacity, and low delay [1, 2]. However, one of the following problems is that these improvements certainly require much more energy supply to drive the widely distributed modules, resulting in massive heat dissipation within a large area [3]. The power dissipation of an individual 5 G base station is about 3700 W, which is $2.5-3$ times larger than a 4 G one, and the discrete heat sources accounts for a large part of the printed circuit boards [4]. Worse still, these stations are usually installed on the top of the building or high in the field, making it impractical to use an active cooling approach owing to the huge operating and maintenance costs. Since the performance and reliability of electronic devices are very sensitive to temperature, the extremely high power dissipation and poor working condition of base stations have made thermal design a great challenge in the development of communication techniques [5–8]. Owing to the benefits of its good performance and easy fabrication, the heat sink is the most widely used cooling method [9, 10]. It is reported that heat sinks make up more than 80% of the thermal management solutions for electronic devices [11]. Among these solutions, heat sinks in natural convection are the most typical, efficient, and economic scheme to enhance the heat transfer of electronic devices.

A great number of efforts have been devoted to the optimization of heat sinks in natural convection due to the high requirements for the heat transfer rate and the compact sink geometry. According to the measured data of different plate heat sinks, Yazicioğlu and Yüncü [12] concluded that the convection transfer rate has an optimal value varying with the heat sink width and height. Tari and Mehrtash [13] numerically studied the effects of the fin distance, sink length, and height on the performance of natural convection heat sinks. They found that as the fin distance increases, the heat transfer rate firstly increases to a peak value, then decreases monotonously. Except for parametric studies, a lot of new schemes of the natural convection heat sinks have been proposed, such as inclined

CONTACT Professor Bing-Yang Cao caoby@tsinghua.edu.cn Key Laboratory for Thermal Science and Power Engineering of Ministry of Education, Department of Engineering Mechanics, Tsinghua University, Beijing 100084, China.

Nomenclature

A	area, m^2
C_k	ratio of the fluid thermal conductivity to solid thermal conductivity, k_f / k_s
C_p	specific heat, J/(kg·K)
DOF	design of freedom
$\mathbf{e}_g$	unit vector in the gravitational direction
g	gravitational acceleration, m/s^2
Gr	Grashof number, $g\beta(\Delta T)_0\rho^2L^3/\mu^2$
H	height, m
h	elevation of the fulid, m
h_m	mesh size, m
k	thermal conductivity, $W/(m \cdot K)$
L	characteristic length, m
p	pressure, Pa
P	modified pressure, Pa
Pr	Prandtl number, $\mu C_p/k$
r_f	filter radius, m
q	heat flux, W/m^2
q_k	convexity parameter for the interpolation of thermal conductivity
q_α	convexity parameter for the interpolation of effective inverse of permeability
Q_s	volumetric heat source, W/m^3
T	temperature, K
TO	topology optimization
U	speed, m/s
$\mathbf{v}$	velocity vector, m/s
W	width, m
$\mathbf{x}$	position vector, m

Greek Symbols

α	effective inverse of permeability
β	coefficient of thermal expansion, 1/K
γ	design variable field
$\tilde{\gamma}$	filtered design variable
$\bar{\tilde{\gamma}}$	projected design variable
η	projection threshold
μ	dynamic viscosity, $kg/(m \cdot s)$
ρ	density, kg/m^3
σ	projection steepness parameter
ϕ	volume constraint on heat sinks
(ΔT)	temperature difference, K

Subscripts

ave	average value
b	heating boundary
d	design domain
f	fluid material
init	initial value
max	maximum value
o	outer surface of the heat sink
ref	reference value for nondimensionalization
s	solid material
0	reference value

Superscripts

i	iteration number
T	transposition
*	dimensionless parameters

fins [14], fins of variable thickness [15], interrupted fins [16] and dual-height fins [17]. The existence of the optimal heat sink design can be interpreted as a tradeoff between increasing the heat transfer area and decreasing the flow resistance of natural convection. Although these size and shape optimization techniques could improve the performance of heat sinks and to some extent reduce the system temperature, the design space is limited to a few geometric parameters, and a priori basic design must be given. As a contrast, topology optimization (TO), which is the science of placing material in an optimum manner respecting predefined objectives and constraints [18], has a much larger number of degrees of freedom (DOF) of design. Its final solution complexity is unconstrained and the optimized designs usually pass over people's expectations [19]. TO can not only help to significantly improve the performance of the design object but also considerably reduce the design time [20]. For a conventional heat conduction optimization problem, the results predicted by TO can be better than those by other optimization methods [21].

TO for heat transfer systems is a young and not robust methodology [19, 22]. The problem becomes more complex when it comes to natural convection, which is a strongly coupled heat transfer process where the variation of the temperature field induces fluid motion under gravity, and the flow filed affects the temperature field by heat convection. To take heat convection into consideration in TO, the usual approach used to interpolate the convective boundaries [23–25]. These researches apply a predetermined effective convection coefficient to simplify the problem, and the method has been used in actual manufacturing [26] and industrial framework [27]. But TO could produce unanticipated designs and closed cavities, which violates the assumptions of the simplified model [28]. The weakness is firstly overcome by Alexandersen et al. [29] by introducing the Brinkman friction term to Navier-Stokes equations, in which they came up with a density-based TO approach for two-dimensional (2 D) natural convection problems without assuming a single constant convection coefficient. Later, Coffin and Maute [30] developed a level-set method which is able to deal with the transient natural convection problems, and the density-based TO method has been extended to the large scale three-dimensional optimization problems with the order of 1×10^8 state DOF [31]. Recently, a reduced-order model governed by simplified physics was

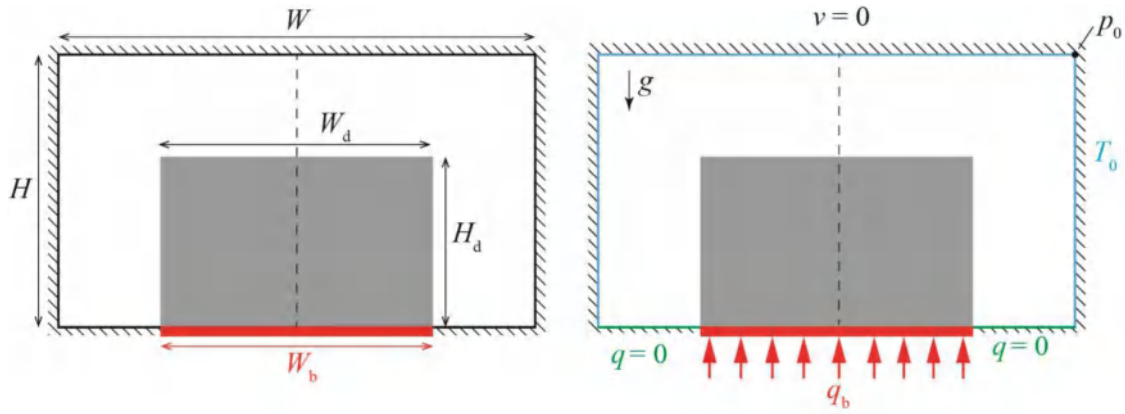

Figure 1. Schematic diagram of the geometries and boundary conditions for the 2 D natural convection heat sink.

proposed to reduce the computational effort [32, 33]. Moreover, TO has been successfully utilized to the design of passive coolers for light-emitting diode lamps, in which the topology-optimized designs yield a 26% lower temperature while 12% less material compared to the common commercial design [34]. Further experimental results demonstrated that topology-optimized heat sinks always perform better than pin-fin heat sinks under the design condition [35, 36]. These studies demonstrate the feasibility of using TO in natural convection problems and provide insights for the design of heat sinks. However, most of the reported work only deals with the small-size heat source cases, in which the heat source is a small part of the design domain boundary and cannot meet the requirement of modern 5 G large-size heat source devices. In addition, the variations of the optimized designs with heat sink volume and material thermal conductivity are still lacking.

In the present work, the optimization of natural convection heat sinks is achieved by the density-based TO method, in which a new gradual parameter scheme is used to avoid the local optima. After determining the reasonable values of mesh size and filter radius, parametric studies are carried out to analyze the dependence of the results with heating power, heat source size, heat sink volume and thermal conductivity ratio of the fluid to solid. The main outline of the obtained heat sink gradually changes from the tree-like structure at the small heating power to the taper structure at the large heating power, verifying the validity of the gradual parameter scheme. The detailed structures significantly change with the heat source size, heat sink volume and thermal conductivity ratio at the small heating power, but the difference weakens as heating power increases. The variation of the results is closely related to the change of the relative strength of convection to heat conduction in natural convection problems. However, two oblique primary branches which connect the bottom and corners of the design domain always exist after TO.

Methodology

The design problem is simplified as a 2 D heat sink subjected to natural convection cooling due to surrounding cold walls, as shown in Figure 1. The gray zone is the design domain where the solid material is freely distributed to form the heat sink, and a flow domain surrounds the heat sink. The upper and side walls are kept at a specified temperature (T_0), and the bottom wall is insulated ($q = 0$), except for the boundary heat flux (q_b) along the bottom of the design domain. A reference pressure p_0 is applied at the corner to ensure a unique solution to the flow equations. With a prescribed constraint on the volume of the heat sink, the objective of the optimization is to minimize the average temperature of the heat flux boundary, corresponding to decrease the heat source temperature in actual devices. The geometry and boundary conditions of the current problem refer to the settings in reference [29], but the heat source size has been increased from $W_b/W_d = 0.05$ (the small size) to $W_b/W_d = 1$ (the large size) to model the situation of 5 G communication base stations, in which the power modules nearly cover the full base plate of the heat sink. It will be displayed that the heat source size does have an impact on the optimization results.

A brief introduction of the density-based TO method will be given in this section. The buoyancy effect is taken into consideration via the Boussinesq approximation, and the Brinkman friction term [37, 38] is introduced to facilitate TO of the flow. More details of the method can be found in references [29, 31].

Governing equations

To simplify the problem, steady, incompressible, laminar, and constant property flows are assumed, and the viscous dissipation is neglected. The resulted Navier-Stokes and convection-diffusion equations with Boussinesq approximation [39] and Brinkman friction term are (dimensionless form):

$$\nabla^* \cdot \mathbf{v}^* = 0 \tag{1a}$$

$$(\mathbf{v}^* \cdot \nabla^*)\mathbf{v}^* = -\nabla^* \cdot P^* + Pr\nabla^* \cdot \left(\nabla^*\mathbf{v}^* + (\nabla^*\mathbf{v}^*)^T\right) - Pr^2 GrT^*\mathbf{e}_g - \alpha\mathbf{v}^* \tag{1b}$$

$$\mathbf{v}^* \cdot \nabla^* T^* - k^*\nabla^* \cdot (\nabla^* T^*) = Q_s^* \tag{1c}$$

The modified pressure, $P = p + \rho gh$, is used to avoid the potential round-off error in numerical calculation of the buoyancy effect. $Pr = \mu C_p/k$ is the Prandtl number that reflects the relative spreading of viscous and thermal effects, and $Gr = g\beta(\Delta T)_0\rho^2L^3/\mu^2$ is the Grashof number that describes the ratio of the buoyancy force to the viscous force in the fluid. Gr can be used to determine the relationship between convection and diffusion and reflects the relative heat source intensity if the solid and fluid materials are determined. For low Gr, the heating power is weak, the flow is dominated by diffusion and heat conduction is the main means of heat transfer. For high Gr, the heating power is strong to excite fast flow, and convection plays a decisive role in the heat transfer.

Topology optimization

TO is originally a discrete 0-1 design problem and naturally has severe numerical instabilities [40]. The basic principle to implement TO is to replace the original discrete optimization problem with the continuous one where the material density is allowed to vary continuously between solid and void [20]. In this paper, an idealized porous material whose permeability and thermal conductivity can vary spatially is assumed to fill the design domain. The limits of very low and very high permeability represent the solid walls with high thermal conductivity and open channels with low thermal conductivity, respectively. This requirement can be realized by the following interpolation functions [29, 31, 41]:

$$\alpha(\gamma) = \alpha_{\max}\frac{1-\gamma(\mathbf{x})}{1+q_\alpha\gamma(\mathbf{x})} \tag{2a}$$

$$k^*(\gamma) = \frac{\gamma(\mathbf{x})[C_k(1+q_k)-1]+1}{C_k\left(1+q_k\gamma(\mathbf{x})\right)} \tag{2b}$$

in which γ is the design variable field that varies continuously between zero and unity, q_α and q_k are the real and positive parameters that tune the convexity of $\alpha(\gamma)$ and $k^*(\gamma)$. Theoretically, the upper bound of α should be infinity to ensure zero velocities in the solid domain, but in numerical simulation, a large finite $\alpha_{\max}$ that sufficiently impedes the flow is used on account of the numerical stability. Equations (2a) and (2b) give $\alpha = \alpha_{\max}$, $k = k^* \times k_f = k_s$ at $\gamma = 0$, and $\alpha = 0$, $k = k_f$ at $\gamma = 1$, as a result, $\gamma = 0$ corresponds to the solid material and $\gamma = 1$ the fluid. In this way, the TO problem has been translated into a problem of finding the best set of the spatially dependent design variable field. The values of q_α and q_k are adjusted to penalize intermediate design variables with respect to the effective inverse of permeability and effective thermal conductivity, respectively, thus driving γ toward the bounds of 0 and 1.

Although the discrete design problem has been converted to a continuous one by Eqs. (2a) and (2b), TO still faces the challenges caused by its ill-posed nature, like checkboards problem, mesh-dependence, and local optimal solution [42]. To further improve the numerical stability, the density filter based on the Helmholtz-type partial differential equation is employed [43], and we have

$$-r_f^*\nabla\tilde{\gamma}^2 + \tilde{\gamma} = \gamma \tag{3}$$

where r_f is the filter radius and $\tilde{\gamma}$ the filtered design variable. An inherent problem of using the density filter method is the gray transition regions between solid and void parts which means the solid/void interfaces in the optimized solutions are not discrete 0/1 transitions but smeared out [44]. This problem can be alleviated by using projection methods [45], and here we use the threshold Heaviside function projection [46]

$$\bar{\tilde{\gamma}} = \frac{\tanh(\sigma\eta) + \tanh(\sigma(\tilde{\gamma}-\eta))}{\tanh(\sigma\eta) + \tanh(\sigma(1-\eta))} \tag{4}$$

where σ, η, $\bar{\tilde{\gamma}}$ denote the projection steepness parameter, the projection threshold, and the projected design variable, respectively. It is important to note that $\bar{\tilde{\gamma}}$ is the physically meaningful material density used in Eqs. (2a) and (2b), and for Figures 2–7 illustrating the optimized structures, it is the distributions of $\bar{\tilde{\gamma}}$ that are shown. The density-based TO method with filtering and projection is also called a three-field approach [18].

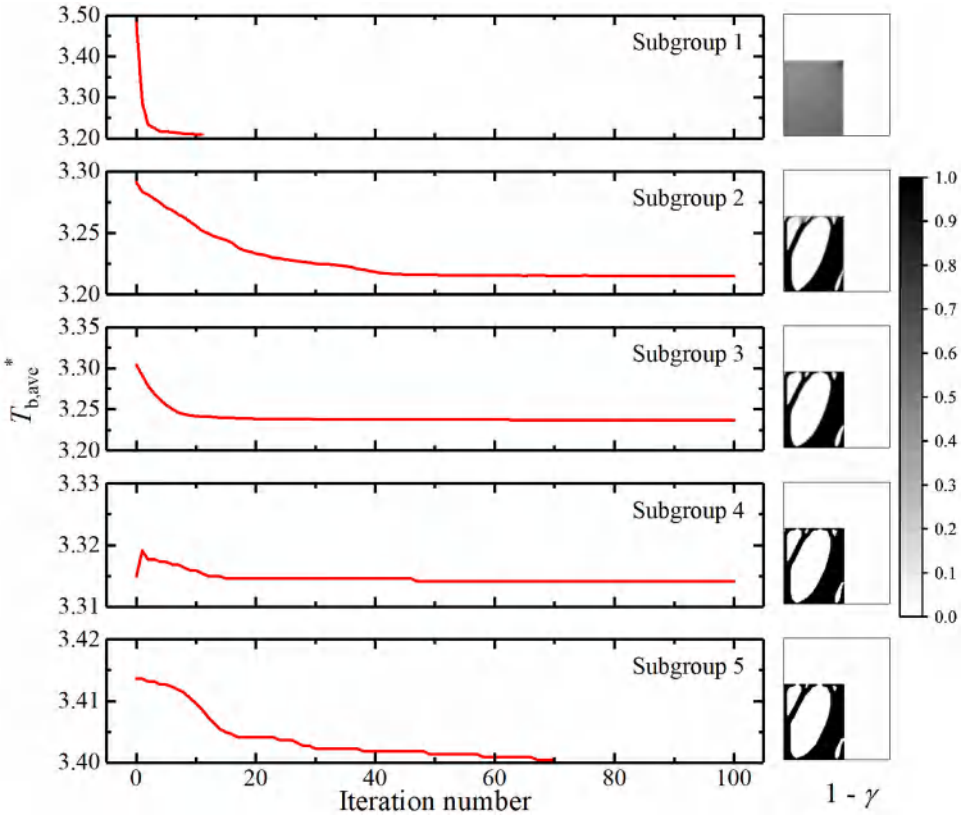

Figure 2. The convergence process for TO at $Gr = 640$. Subgroup 1 to 5 refers to the different parameters of interpolation and projection in Eqs. (5). The gray-scale map refers to the solid material distribution $1 - \gamma$. The values of $T^*_{b,ave}$ are calculated during the optimization process using the Brinkman friction term.

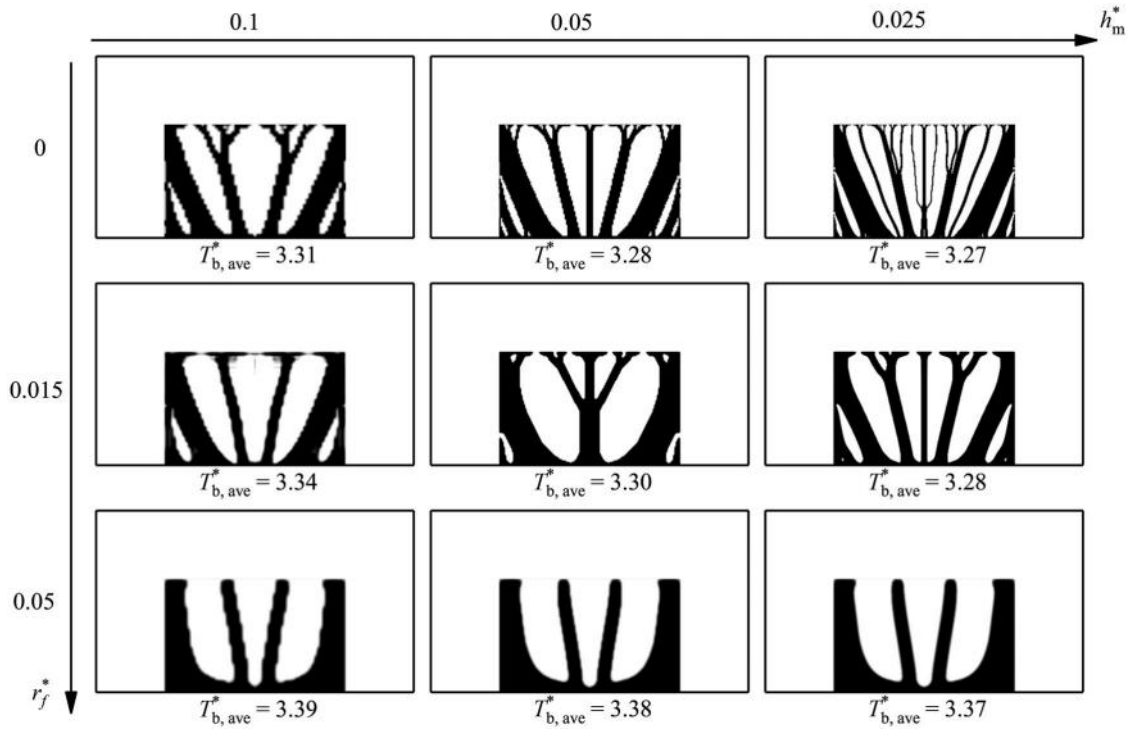

Figure 3. Topology-optimized designs varying with the dimensionless mesh size (h^*_m) and filter radius (r^*_f) at $Gr = 640$. The black regions represent the heat sink (solid material) and the white regions the open channel (fluid material).

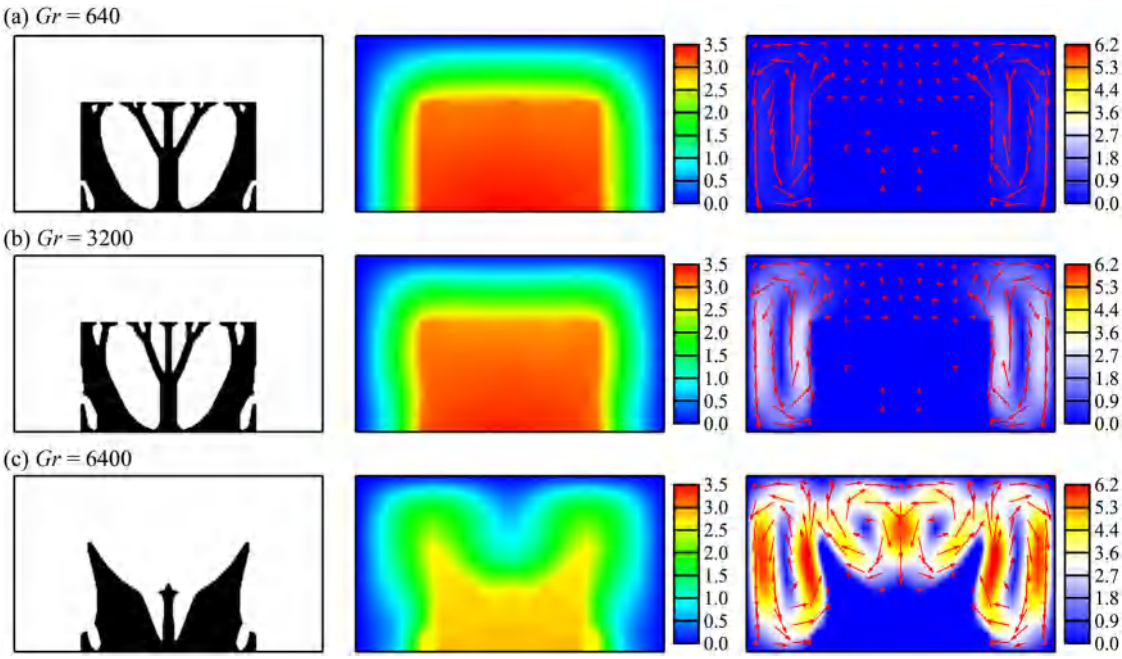

Figure 4. Designs, temperature fields, and velocity fields obtained by TO varying with *Gr*. Temperatures and velocities are nondimensionalized. For different *Gr*, the velocity vectors (arrows) are normalized by dividing the corresponding maximum velocity ($\bar{\mathbf{v}} = \mathbf{v}^*/v^*_{\max}$).

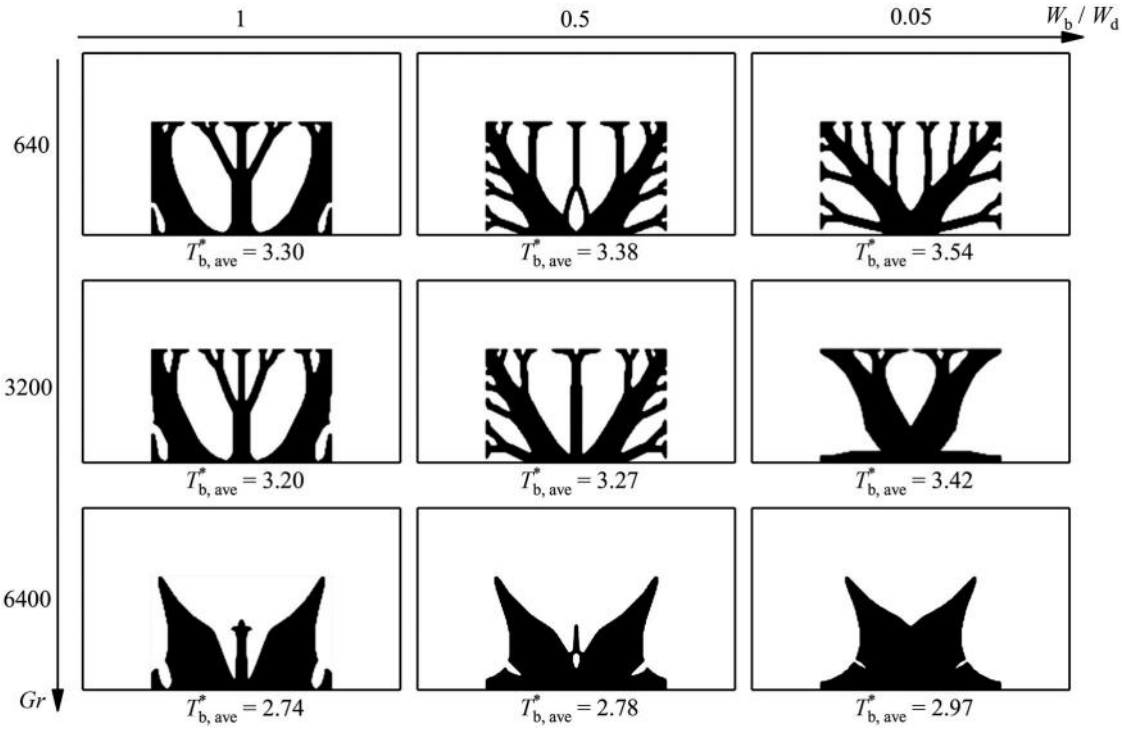

Figure 5. Designs obtained by TO for different heat source sizes (W_b / W_d). The heat sink volume and thermal conductivity ratio are $\phi = 0.5$ and $C_k = 10^{-2}$.

Numerical solution

The solution of the TO problem involves the following procedures: **(1) Discretization and initialization**. The finite element method is employed to numerically solve the governing equations. The initial design is $\gamma_{\text{init}} = 1 - \phi$ where ϕ is the volume constraint on heat sinks defined as $\int \bar{\bar{\gamma}}(\mathbf{x})dA \leq \phi A_d$. (2) **System reanalysis**. For a given design variable distribution,

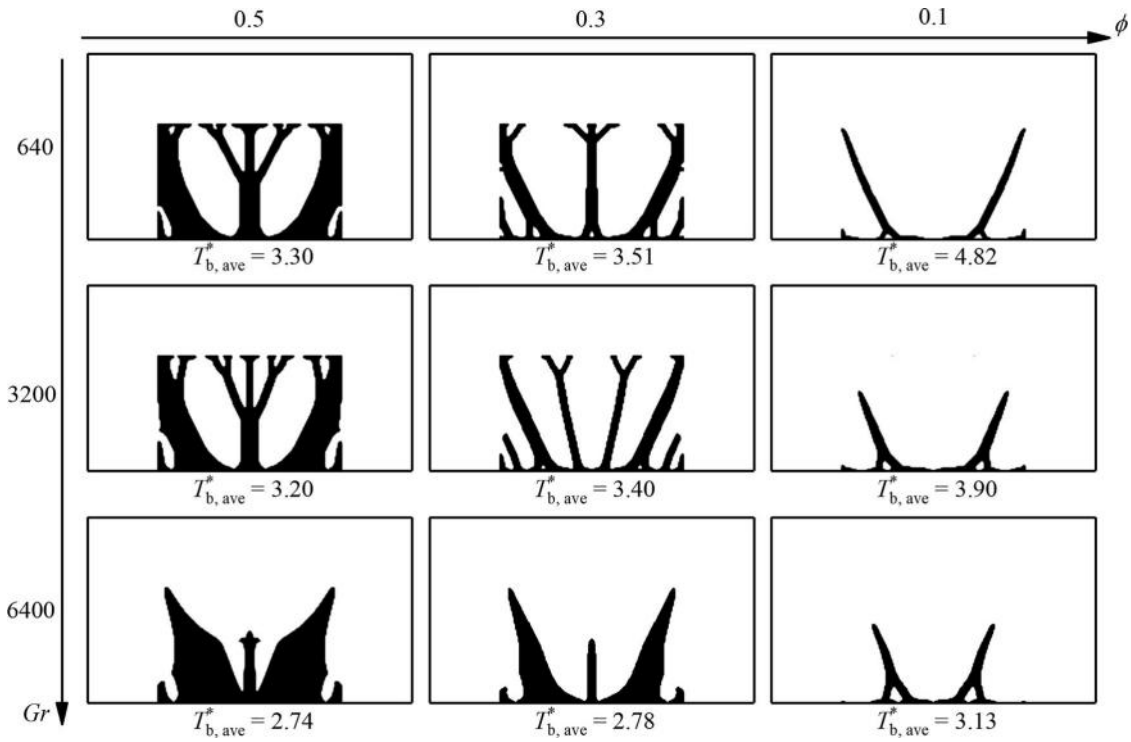

Figure 6. Designs obtained by TO for different heat sink volumes (ϕ). The heat source size and thermal conductivity ratio are $W_b / W_d = 1$ and $C_k = 10^{-2}$.

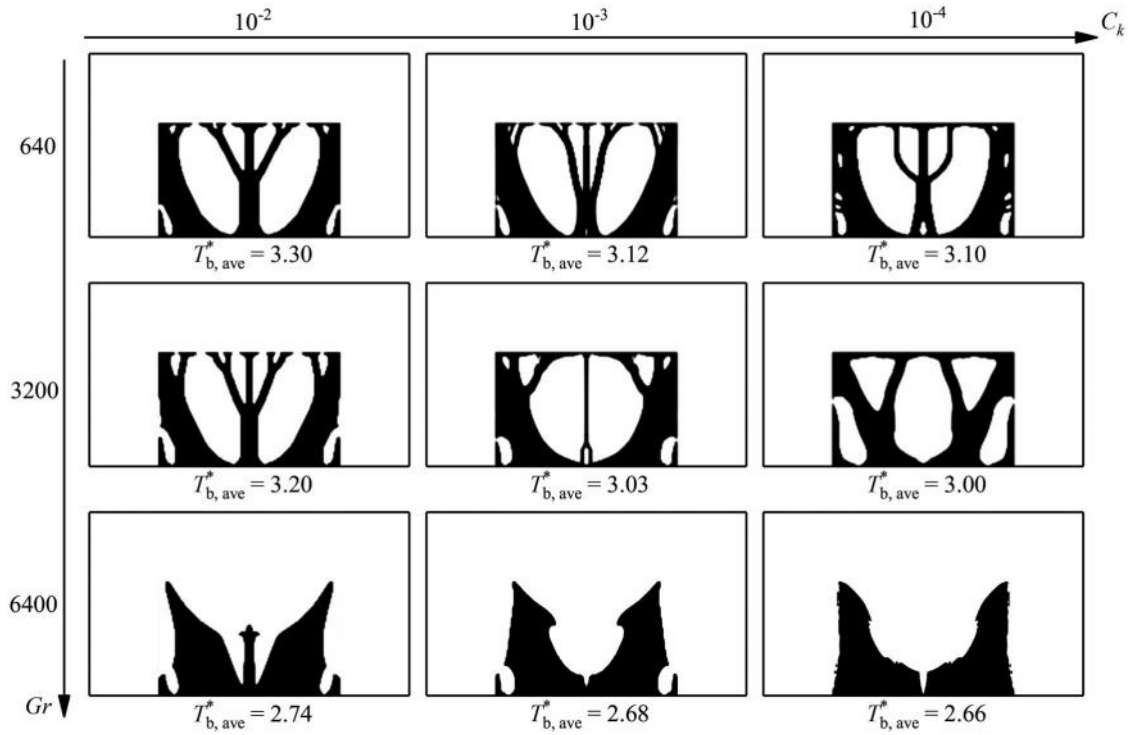

Figure 7. Designs obtained by TO for different thermal conductivity ratios (C_k). The heat source size and heat sink volume are $W_b / W_d = 1$ and $\phi = 0.5$.

the damped Newton method with a constant and empirically determined damping factor is utilized to solve Eqs. (1a) - (1c). The effective inverse of permeability and effective thermal conductivity are interpolated using Eqs. (2a) and (2b), and the velocity field and temperature field are obtained. **(3) Sensitivity**

Table 1. Dimensionless average temperature of the heat source for different designs varying with *Gr*. Considering the symmetry, only the right half-plane of the designs is drawn. The bold number denotes the best performance for the same flow condition (row).

	$T^*_{b,ave}$		
	Design 1	Design 2	Design 3
	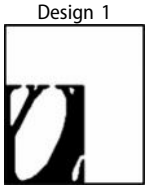	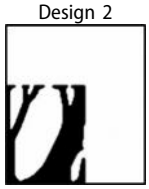	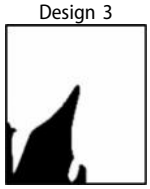
Gr			
640	**3.30**	3.32	3.92
3200	3.20	**3.20**	3.34
6400	2.97	2.96	**2.74**

Note: designs 1 – 3 are given by TO for $Gr = 640$, 3200, 6400 where the heat source size is $W_b/W_d = 1$.

analysis. In order to use gradient-based optimization algorithms to the TO problem, the adjoint method [20] is adopted to calculate the sensitivities, which refer to the gradients of the objective function and constraint functions to the design variables. **(4) Regularization.** The design field is filtered and projected by Eqs. (3) and (4). **(5) Optimization (material redistribution).** The well-known method of moving asymptotes [47] is employed since it is especially compatible with TO problems. **(6) Convergence judgment.** Repeating steps (2) - (5) unless the convergence criterion is satisfied. In practice, the stopping criteria is $\|\gamma^i - \gamma^{i-1}\|_\infty \leq 0.01$ or the iteration number denoted as superscript i reaches a maximum value of 100.

More importantly, a gradual increasing scheme for the parameters of interpolation and projection is performed:

$$q_k = \{10^{-1}, 10^0, 10^1, 10^2, 10^3\} \tag{5a}$$

$$q_\alpha = \{10^1, 10^1, 10^2, 10^2, 10^3\} \tag{5b}$$

$$\alpha_{max} = \{10^5, 10^5, 10^5, 10^6, 10^7\} \tag{5c}$$

$$\sigma = \{1, 1, 1, 5, 10\} \tag{5d}$$

The four parameters are changed at intermediate stages of convergence. The sequences are chosen to stabilize the optimization process and produce better results. The small values at the beginning result in a more convex optimization problem and alleviate premature convergence to poor local optima, while the increasing values gradually penalize the intermediate design variables and force the design variables toward 0 and 1. It should be noted that the results of such non-linear optimization problems are highly dependent on the initial design and the solving process. Compared with the increasing scheme in reference [29], our scheme yields stronger linearity of the thermal conductivity interpolation at the initial phase, and gradually cuts down the linearity of the inverse of permeability interpolation. These settings are expected to improve the performance of the optimized results. The projection threshold is fixed at $\eta = 0.5$.

Results and discussion

For the design problem shown in Figure 1, the geometric parameters are $H = 4$ m, $W = 7$ m, $H_d = 2.5$ m, $W_d = W_b = 4$ m. The cold wall temperature and corner point pressure are $T_0 = 0$ K and $p_0 = 0$ Pa. The properties of the fluid material are $\rho_f = 1\,kg/m^3$, $k_f = 1\,W/(m \cdot K)$, $C_{p,f} = 1\,J/(kg \cdot K)$, $\mu = 1\,kg/(m \cdot s)$ and $\beta = 1\,K^{-1}$. The solid material is set to have the same density and specific heat as the fluid material, and its thermal conductivity is $k_s = 100\,W/(m \cdot K)$ unless otherwise stated. Thus, we have $Pr = 1$ and $C_k = 0.01$. The *Gr* is calculated by taking the height of the entire domain (H) as the characteristic length, and the reference temperature difference is calculated as $(\Delta T)_0 = q_b W_b/(k_f q_b^*)$, in which $q_b^* = 0.22$ is a pre-determined dimensionless heat flux. Three values of the heating power density $q_b = 5.5/2.75/0.55\ W/m^2$ are investigated, corresponding to $Gr = 640/3200/6400$. In this way, the physical settings are consistent with those in the literature [29], so the present TO results for the large-size heat source ($W_b/W_d = 1$) can be directly compared to the previous ones for the small-size heat source ($W_b/W_d = 0.05$). For the sake of comparison, the results are non-dimensionalized as $L^* = L/L_{ref}$, $T^* = (T - T_{ref})/(\Delta T)_0$ and $v^* = v/U_{ref}$, in which $L_{ref} = 1$ m is the reference length scale, $T_{ref} = 0$ K is the reference temperature and $U_{ref} = k_f/(C_{p,f}\ \rho_f\ L_{ref})$ is the reference velocity.

Eqs. (1) are solved by the laminar conjugate heat transfer module of COMSOL Multiphysics with a square finite element. According to reference [48], the transition from laminar to turbulent flow usually happens around $Gr = 10^9$ for natural convection in large space, and $GrPr = 5 \times 10^4$ for natural convection in horizontal interlayers. However, the transition criteria are not suitable for the complex and changing geometries produced during the process of TO. For specific problems, experimental studies are required, but it is beyond the scope of this work.

Convergence and mesh-independence check

At first, the numerical convergence of the TO method is checked. The optimization process for TO at

$Gr = 640$ is shown in Figure 2, in which the dimensionless temperature objective functions ($T^*_{b,ave}$) varying with the iteration number in every subgroup of the advancing parameters are depicted. Moreover, the material distribution results (1 - γ) of each subgroup are displayed. The values of $T^*_{b,ave}$ are calculated by the optimization program, which use the Brinkman friction term to model the solid region as shown in Eq. (1b). The black and white regions in the gray-scale map represent the heat sink (solid material) and the open channel (fluid material), respectively. The heat sink volume constraint (ϕ), dimensionless mesh size ($h^*_m = h_m/L_{ref}$) and dimensionless filter radius (r^*_f) are 0.5, 0.05 and 0.015, respectively. The initial material distribution $1 - \gamma = \phi$ corresponds to a uniform gray distribution of the design variable field and is not shown in Figure 2. For parameter subgroup 1 and 5, the convergence criterion is satisfied during the iteration. For the other subgroups, the iteration numbers reach the maximum value of 100. During the optimization process of each subgroup, the objective function decreases at first and becomes a nearly constant line afterward, indicating that the objective function has converged when the parameters change. The material distributions show how 1 - γ varies from the initial uniform design to a final tree-like design. The main outline of the heat sink has been determined after the optimization process of subgroup 2, emphasizing the importance of using a slight penalization at the beginning. The remaining optimization processes gradually penalize the intermediate value of γ, adjust the allowed minimal length scale, and finally result in a discrete design.

Then, TOs for different h^*_m and r^*_f at $Gr = 640$ are conducted to determine reasonable mesh size and intensity of the density filter, so that the optimization program could produce designs that will not change remarkably as the mesh size decreases. The heat sink designs predicted by TO varying with h^*_m and r^*_f are drawn in Figure 3. At $Gr = 640$, the buoyancy force is very weak and the fluid should be almost at rest state, thus, the results of TO for pure heat conduction problems can be termed as a benchmark. To avoid the possible errors caused by employing the Brinkman friction term, $T^*_{b,ave}$ in Figure 3 are calculated by choosing $\gamma = 0.5$ as the solid-to-fluid interface and setting the solid and fluid regions in COMSOL Multiphysics. For $h^*_m = 0.05$ and $r^*_f = 0.015$, the converged value of $T^*_{b,ave}$ is 3.40 in Figure 2, but the re-calculated value is 3.30 in Figure 3, the deviation originates from the Brinkman friction term. Without special explanations, the following presented values of $T^*_{b,ave}$ are all the re-calculated ones, not the converged ones.

The solid materials in Figure 3 all distribute in a tree-like way to connect the bottom heat source and the edges of the design zone via some upward branches. As the primary branches from the bottom stretch into the design domain, they will diverge into several thin secondary branches. The tree-like design is similar to the typical TO results for pure conductive heat transfer problems [49]. As the mesh size decreases, the minimal length scale allowed in the optimized design decreases, which leads to more small-scale structures and lower temperature, and hinders the mesh convergence. In the results of $r^*_f = 0$, a growing number of secondary branches and tiny holes appear as h^*_m reduces from 0.1 to 0.025, and $T^*_{b,ave}$ decreases from 3.31 to 3.27, exhibiting a strong mesh-dependence. The density filter technique improves the mesh-convergence by imposing control over the length scale, but it sacrifices some optimization effects. When h^*_m is fixed, the tiny structures on the top of the design domain disappear as r^*_f increases from 0 to 0.015, while the bottom thick structures are remained and $T^*_{b,ave}$ are raised. When r^*_f goes to 0.05, the density filter is so strong that the three mesh sizes result in the same heat sink designs, and the almost equal objective values ($T^*_{b,ave} = 3.39, 3.38, 3.37$) verifies the mesh-independence of solving the governing equations. Figure 3 validates the effectiveness of the density filter approach. In this work, $h^*_m = 0.05$ and $r^*_f = 0.015$ are chosen since they have a moderate mesh-independence and calculation efficiency. The value of the filter radius also agrees with that in reference [29]. A larger filter radius can guarantee stronger mesh-independence, but it is supposed to impair the effect of TO. It is worth noting that the designs in Figure 3 have distinct solid-fluid interfaces, confirming that the gray transition regions originating from the filter technique have been successfully suppressed by the projection method.

Effects of grashof number

Using the numerical parameters determined above, the topology optimized designs for different heating powers are shown in Figure 4, in which the temperature and velocity distributions are also illustrated. In general, all designs have reached the upper bound of the volume constraint, which means the heat sink makes up 50% of the design domain, but the topology optimized heat sink structures, as well as temperature and velocity fields, vary with Gr. For $Gr = 640$, the

tree-like heat sink quickly transfers heat from the heat source to surrounding regions, causing a nearly uniform temperature distribution in the design domain. In the fluid domain, the dimensionless velocities are less than one and the temperature profile is diffusive, demonstrating that heat conduction is the main way of heat transfer. When Gr increases to 3200, the obtained design is very similar to that of $Gr = 640$. There are also three primary branches extending from the heat source to the top and side edges of the design domain, and they diverge at the ends. Only a few tiny changes in size are observed, like the expansion of voids on the top. However, the speed of the fluid flow is increased and heat convection is strengthened. There are two vortices on the sides of the design domain, raising the maximum dimensionless velocity to be about 3. The temperature profile at the bottom has deviated from the diffusive one. As Gr further increases to 6400, the optimized design changes remarkably. The middle primary branch no longer stretches into the top edge of the design domain. The oblique primary branches thicken at the bottom and thin at the top, and the secondary branches at the ends disappear. In this case, the fluid flow forms four evident vortices and the maximum dimensionless velocity increases to be more than 6. The temperature distribution is not uniform in the design domain, but the maximum dimensionless temperature decreases to be less than 3, indicating that the heat transfer has been adequately enhanced by heat convection. Although TO gives different heat sink designs for different heating power, their common characteristic is that the heat sinks cover the whole heat source and has three primary branches.

To test the performance of TO, the cooling capacity of different heat sink designs in Figure 4 are compared under different flow conditions, as Table 1 shows. The design optimized for a certain flow condition has the lowest heat source average temperature (the bold numbers) for its particular flow condition, and performs better than the other designs. Take $Gr = 640$ as an example, TO for $Gr = 640$ gets $T^*_{\mathrm{b,ave}} = 3.30$, which is lower than that for $Gr = 3200$ ($T^*_{\mathrm{b,ave}} = 3.32$) and $Gr = 6400$ ($T^*_{\mathrm{b,ave}} = 3.92$). One special case is $Gr = 3200$ where the structure optimized at $Gr = 640$ still has the lowest average temperature, but it is not surprising considering the structure is very similar to that optimized at $Gr = 3200$. Table 1 verifies the validity of the TO method for natural convection heat sinks with a large-size heat source.

The variation of the optimized design can be interpreted as the harmony of increasing heat transfer area and decreasing flow resistance. Heat sinks play the role of building high-thermal-conductive paths which shorten the effective distance of the heat source and surrounding cold environment, but the effect is closely related to the strength of convection and heat conduction, especially for the highly-coupled natural convection. When the surface area of the heat sink broadens, on one hand, the contact area between the solid and fluid expands, which is beneficial to enhance the heat conduction; on the other hand, the flow resistance also increases, which will depress the heat convection. When the heating power is small, heat conduction is the main way of heat transfer in the fluid regions. The influence of the flow resistance can be ignored, and the heat sink will form a shape that contacts with the fluid as much as possible. So, TO at $Gr = 640$ prefers to produce the tree-like heat sink that has a large surface-to-volume ratio, and the heat sink will cover the whole heat source to make sure that all heat generated can be efficiently conducted. As the heating power intensifies, the convection begins to take effect but its contribution to heat transfer has not significantly exceeded heat conduction. The tree-like structure coincidently has two oblique primary branches which provide smooth vertical surfaces to motivate flow, making it nearly the optimized design at $Gr = 3200$ as well. When the heat source is strong enough, convection dominates heat transfer. In this case, the shape of the branches will be modified to better accommodate to the strong flow and reduce the flow resistance. Therefore, in the optimized design for $Gr = 6400$, tiny secondary- and tertiary- branches vanish and the remained primary branches form the taper structures, which improve the heat conduction at the bottom slow flow regions and adapt to the fast flow at the top and side. As a validation, the area of the heat sink's outer surface A_o is calculated, which is defined as the solid-to-fluid surface except for the enclosed fluid pockets. For the 2 D problem, the dimension perpendicular to the paper is set as 1 m, and the values of A_o for $Gr = 640$, 3200 and 6400 are 28.2 m^2, 30.6 m^2 and 16.2 m^2, respectively. The optimized structures at $Gr = 640$ and 3200 are very similar, so they have almost the same outer surface area. The small increase of less than 10% as Gr varies from 640 to 3200 can be interpreted as the non-uniqueness of the TO results. However, for $Gr = 6400$, A_o of the optimized structure is significantly reduced by nearly 50%, quantitatively demonstrating that TO prefers to

produce less complex structure in the convection dominant regime.

Effects of heat source size

Except for the *Gr* that reflects the heating power, the heat source size is another factor that we care about. TOs for different heat source sizes are conducted and the results are shown in Figure 5. For the same *Gr*, the heating power density has been changed to keep the heating flow as a constant. The results for $W_b/W_d = 0.05$ do a good job of matching the results in reference [29], validating the new parameter advancing scheme again. It can be found that the topology-optimized designs regularly vary from the tree-like structure at the small *Gr* to the taper-like structure at the large *Gr*, but the location of the primary branches and direction of the secondary branches are different. At $Gr = 640$, as the heat source size cuts down, the vertical primary branch originating from the center of the heat source fades away and many secondary branches extend upward from the two oblique primary branches. At $Gr = 6400$, similar variation trend with the heat source size is observed, the distribution of the solid material moves toward the symmetry line. At $Gr = 6400$, the three designs all have the taper structure whose vertices are at the corner of the design domain, the little difference is the degree of separation of the primary branches and gaps of the surface. In addition, $T^*_{b,ave}$ for the same *Gr* increases as the heat source size reduces.

The effect of heat source size reflects the change of major heat dissipation path. In the case of $W_b/W_d = 1$, the heating power is distributed in a large area. The distance from the heat source to the side wall and the top wall is $(W^* - W^*_d)/2 = 1.5$ and $H^* = 4$, of which the former is less than half of the latter. As a result, enhancing lateral heat transfer gains more than enhancing upward heat transfer, and the topology-optimized designs will distribute a large quantity of the solid material toward the side wall. As the heat source size cuts down to $W_b/W_d = 0.5$, the distance from the heat source to the side wall increase, the superiority of lateral heat dissipation is diminished, making TO form more upward branches. In the case of $W_b/W_d = 0.05$, the length of the lateral heat dissipation is $(W^* - 0.05W^*_d)/2 \approx 3.5$, which has already been comparable to the length of the upward heat dissipation. Since upward heat transfer plays the same role as the lateral heat transfer, the primary branch predicted by TO grows along the diagonal line of the half plane, and the solid material is distributed more evenly in direction. Moreover, the reduction of heat source size improves the localization of high temperature hot spots, making the heat dissipation more difficult. Thus, $T^*_{b,ave}$ of the optimized design will increase as the heat source size decreases.

The influence of the heat source size is noticeable at the small *Gr* but declines with *Gr* increasing, which can be attributed to the change of the relative strength of convection to heat conduction, too. In the heat conduction dominant regime, the root of the tree-like heat sink is the heat source. Consequently, there are more primary branches directly growing from the heat source as its size increases at $Gr = 640$. In the convection dominant regime, the design direction is to prompt fast flow and reduce flow resistance at the same time. As a consequence, the taper-like heat sink which could excite four vortices is the best choice at $Gr = 6400$, no matter how much the heat source size is. However, the tendency of the solid material to gather toward the symmetry remains. In the intermediate heat transfer regime, the benefits of increasing the heat transfer area and decreasing the flow resistance are at the same order; hence the optimized design will lie between the tree-like structure and the taper-like one.

Effects of heat sink volume

Previous studies are all based on $\phi = 0.5$, which could probably be difficult to achieve in actual devices owing to the limited design space. To better understand the characteristics of TO for natural convection heat sinks, two lower volume constraints are further considered, of which the obtained results are shown in Figure 6. For $\phi = 0.3$, the allowed volume of the heat sink is still large and the design varies with *Gr* in the same way as $\phi = 0.5$, from the tree-like structure with many branches at $Gr = 640$ to the taper structure with gradient thickness at $Gr = 6400$. But the thickness of the branches is clearly shown to be thinner for the same *Gr*. When ϕ decreases to 0.1, the thinning effects are more pronounced. The provided solid material is only able to construct two oblique primary branches and other branches disappear, causing the outlines of the heat sink nearly remain the same when *Gr* varies from 640 to 6400, but they still reflect the intensifying of the convection strength. At $Gr = 640$, the primary branches are thinner and longer, because the optimized design in the conduction dominant regime should stretch into the design domain as much as possible. As the convection intensifies, the

primary branches become shorter and thicker to adapt to the fluid flow. Owing to the lack of solid material, the heat sink cannot cover the whole heat source and there are barely secondary branches even at small Gr, but heat from the bottom heat source will be comfortably conducted away with the help of the oblique branches, which is favorable to reduce the temperature of the heat source. The results of $\phi = 0.1$ reveal that for the present heat sink design problem, constructing two oblique branches to connect the bottom heat source and the corners of the design domain is always the most effective way to improve the heat dissipation.

In addition, the heat source average temperature also decreases as the heat sink volume reduces, since the strengthening effect of the high thermal conductivity solid material on heat transfer is weakened. However, the effect of the heat sink volume diminishes as Gr increases. At $Gr = 640$, the dimensionless temperature rise of the heat source is 1.52 as reduces from 0.5 to 0.1. But at $Gr = 3200$ and 6400, the dimensionless temperature rises are 0.70 and 0.39, respectively. Along with the variation of the heat sink structure, it is concluded that the results of TO is sensitive to the heat sink volume in the conduction dominant regime, but the sensitivity decreases as heat convection enhances.

Effects of thermal conductivity ratio

Another physical parameter that may affect the optimization results is the thermal conductivity ratio C_k. The above optimizations are conducted at $C_k = 10^{-2}$ since it is an often-used setting in the TO problem of natural convection [29, 31–33]. However, for practical heat sinks, the common solid material is aluminum or copper, and the fluid is air, resulting in $C_k \approx 1/9000$ or 1/15000. To investigate the influence of C_k, TOs of $C_k = 10^{-3}$ and 10^{-4} are also carried out and the results are shown in Figure 7. When C_k varies, only the thermal conductivity of the solid material is changed in the optimization calculation. It is found that a smaller C_k does not qualitatively influence the variation tendency of the optimized designs, they still vary from the tree-like structure at $Gr = 640$ to the taper structure at $Gr = 6400$, but the details of the heat sink change dramatically. Take $C_k = 10^{-3}$ as an example, the optimized design at $Gr = 640$ has a thick vertical primary branch, from which several secondary branches stretch. When Gr increases to 3200, the vertical primary branch becomes significantly thinner and there are no secondary branches on it. At $Gr = 6400$, the middle branches vanish, leaving a large open hole around the center of the design domain. For $C_k = 10^{-4}$, the same disappearance process of the middle branches has been observed.

However, for a fixed Gr, different C_k causes the optimized designs and objective temperature functions to be different, and the effect of C_k weakens as Gr increases. At $Gr = 640$ where heat conduction dominates the heat transfer, the secondary branches in the tree-like structures become thinner and more white holes appear as C_k decreases. Because a smaller C_k means the solid material has higher thermal conductivity, a smaller cross-section area is required to conduct a particular heat rate through it. This finding is consistent with that reported in TO of pure heat conduction problems [49]. The reduction of $T^*_{\mathrm{b,ave}}$ is 0.2 as C_k decreases from 10^{-2} to 10^{-4}. At $Gr = 3200$, heat convection enhances but heat conduction still acts on the same order of magnitude as convection. As C_k declines, the heat is conducted to the fluid more efficiently via the heat sink, inducing the flow to be faster. TO still predicts the tree-like structure with large area side faces that is beneficial to both conduction and convection and the reduction of $T^*_{\mathrm{b,ave}}$ is still 0.2, but the middle vertical branches that impede flow fades away. At $Gr = 6400$, reducing C_k nearly has no impact on the optimized structure except for the disappearance of the middle vertical branches. In the convection dominant regime, adapting to the flow is prior to enhancing heat conduction. Thus, TO obtains the similar taper structure for different C_k. The optimized $T^*_{\mathrm{b,ave}}$ reduces as C_k decreases, indicating the improvement of heat transfer caused by higher thermal conductivity of the solid material, but the decreasing amplitude is only 0.08. Figure 7 suggests that although the analyses of heating power and heat source size are based on the results of $C_k = 0.01$, they are still inspirable to the design of actual aluminum-air or copper-air heat sinks.

Conclusions

In this paper, the density-based TO method with filter and projection techniques is utilized to achieve the 2 D TO design of natural convection heat sinks. A new gradual parameter scheme is proposed to avoid too rapid convergence to local optima, and an explicit mesh-independence check is conducted to determine reasonable values of the mesh size and filter radius. These settings result in an easy-to-use and robust TO method for the design of natural convection heat sinks. The heat sink optimized for a certain flow condition is proved to have better heat dissipation

performance than the others for its particular flow condition, verifying the validity of the TO method.

Parametric studies are carried out to investigate the effects of four physical factors. The obtained design gradually changes from the tree-like structure to the taper structure as *Gr* that represents the relative heating power increases, but the location, direction, thickness, and number of the branches are different for different heat source sizes, heat sink volumes and thermal conductivity ratios, and the impact of the three factors weakens with *Gr* increasing. For a small *Gr* which corresponds to the relatively small heating power, more primary branches stretch out from the heat source as the heat source size broadens, thickness of the branches thins as the heat sink volume reduces, and number of the fluid holes grows as the solid material thermal conductivity rises. For a large *Gr*, the optimized designs generally form the taper structure with few secondary branches, regardless of the heat source size, heat sink volume and thermal conductivity ratio. For an intermediate *Gr*, the optimized design lies between the tree-like structure and the taper structure. Among the large number of optimized designs, two oblique primary branches connecting the bottom and top corners of the design domain are the common feature.

The dependence of the optimized design on heating power, heat source size, heat sink volume and thermal conductivity ratio is related to the variation of dominant heat transfer way in natural convection. In the heat conduction dominant regime, the heat sink will try to cover the whole heat source and form a shape that contacts with the fluid as much as possible. Therefore, TO will end up with a tree-like structure whose branching ways are sensitive to the other physical conditions. In the convection dominant regime, fluid flow is so strong that the taper heat sink which could motivate flow without introducing too much flow resistance is preferred by TO, regardless of the other physical conditions. For the current geometry, since the oblique primary branches effectively reduce heat accumulation at the heat source, they always exist in the optimized designs.

Disclosure statement

No potential conflict of interest was reported by the authors.

Funding

This work is financially supported by National Natural Science Foundation of China [Nos. U20A20301, 51825601] and ZTE Research Fund.

Notes on contributors

Han-Ling Li is a Ph.D. student at the School of Aerospace Engineering, Tsinghua University. He received his B.S. in the Department of Engineering Mechanics from Tsinghua University. He is currently working on the multi-scale simulation and optimization of heat transfer in electronic devices.

Dai-Yan Lan is a senior system engineer in thermal design reliability department, ZTE Corporation. He is mainly responsible for the thermal design of wireless base stations, including AAU, RRU, and pRRU.

Xian-Ming Zhang is the leader of thermal design expert group of ZTE Corporation. His main job is the planning of thermal design and the application of new technologies for the products of ZTE Corporation.

Bing-Yang Cao is a Professor of School of Aerospace Engineering, Tsinghua University. His research interests cover heat transport and thermophysical properties of nanostructures, thermal functional materials, advanced thermal management technologies. He has published over 150 SCI-indexed journal papers and won the New Century Excellent Talents of MOE (2011), Zhonghua-Wu Outstanding Young Scholar Award of CSET (2014), Outstanding Young Scientist Award of NSFC (2018), First Natural Science Prize of MOE (2019). He serves as Editor-in-Chief of ES Energy & Environment, editorial board member of Journal of Physics: Condensed Matter, Scientific Reports, and PLoS One.

References

[1] N. Marchetti, "Towards 5th generation wireless communication systems," *ZTE Commun.*, vol. 13, no. 1, pp. 11–19, 2015. DOI: 10.3969/j.issn.1673-5188.2015.01.002.

[2] V. C. M. Leung and Z. Haijun, "Ultra-dense networking architectures and technologies for 5G," *ZTE Commun.*, vol. 16, no. 2, pp. 1–2, 2018. DOI: 10.3969/j.issn.1673-5188.2018.02.001.

[3] A. Fisusi, D. Grace and P. Mitchell, "Energy saving in a 5G separation architecture under different power model assumptions," *Comput. Commun.*, vol. 105, pp. 89–104, Jun. 2017. DOI: 10.1016/j.comcom.2017.01.010.

[4] T. K. Hotta and S. P. Venkateshan, "Optimal distribution of discrete heat sources under natural convection using ANN–GA Based Technique," *Heat Transfer Eng.*, vol. 36, no. 2, pp. 200–211, 2015. DOI: 10.1080/01457632.2014.909222.

[5] M. Pedram and S. Nazarian, "Thermal modeling, analysis, and management in VLSI circuits: Principles and methods," *Proc. IEEE*, vol. 94, no. 8, pp. 1487–1501, 2006. DOI: 10.1109/JPROC.2006.879797.

[6] S. V. Garimella, T. Persoons, J. A. Weibel and V. Gektin, "Electronics thermal management in information and communications technologies: challenges and future directions," *IEEE Trans. Compon., Packag. Manufact. Technol.*, vol. 7, no. 8, pp. 1191–1205, 2017. DOI: 10.1109/TCPMT.2016.2603600.

[7] Y. C. Hua, H. L. Li and B. Y. Cao, "Thermal spreading resistance in ballistic-diffusive regime for GaN HEMTs," *IEEE Trans. Electron Dev.*, vol. 66, no. 8, pp. 3296–3301, 2019. DOI: 10.1109/TED.2019.2922221.

[8] D. S. Tang, G. Z. Qin, M. Hu and B. Y. Cao, "Thermal transport properties of GaN with biaxial strain and electron-phonon coupling," *J. Appl. Phys.*, vol. 127, no. 3, pp. 035102, Jan. 2020. DOI: 10.1063/1.5133105.

[9] M. Yang and B. Y. Cao, "Numerical study on flow and heat transfer of a hybrid microchannel cooling scheme using manifold arrangement and secondary channels," *Appl. Therm. Eng.*, vol. 159, pp. 113896, Jun. 2019. DOI: 10.1016/j.applthermaleng.2019.113896.

[10] B. M. Nafis, R. Whitt, A. Iradukunda and D. Huitink, "Additive manufacturing for enhancing thermal dissipation in heat sink implementation: A review," *Heat Transfer Eng.*, vol. 42, no. 12, pp. 2021, in press. DOI: 10.1080/01457632.2020.1766246.

[11] C. M. A. Kumar and P. C. M. Kumar, "Review on electronics cooling systems," *Adv. Nat. Appl. Sci.*, vol. 11, no. 8, pp. 271–279, 2017.

[12] B. Yazicioğlu and H. Yüncü, "Optimum fin spacing of rectangular fins on a vertical base in free convection heat transfer," *Heat Mass Transfer*, vol. 44, no. 1, pp. 11–21, 2007. DOI: 10.1007/s00231-006-0207-6.

[13] I. Tari and M. Mehrtash, "Natural convection heat transfer from inclined plate-fin heat sinks," *Int. J. Heat Mass Transf.*, vol. 56, no. 1–2, pp. 574–593, 2013. DOI: 10.1016/j.ijheatmasstransfer.2012.08.050.

[14] M. Fujii, "Enhancement of natural convection heat transfer from a vertical heated plate using inclined fins," *Heat Trans. Asian Res.*, vol. 36, no. 6, pp. 334–344, 2007. DOI: 10.1002/htj.20168.

[15] D. K. Kim, "Thermal optimization of plate-fin heat sinks with fins of variable thickness under natural convection," *Int. J. Heat Mass Transf.*, vol. 55, no. 4, pp. 752–761, 2012. DOI: 10.1016/j.ijheatmasstransfer.2011.10.034.

[16] M. Ahmadi, G. Mostafavi and M. Bahrami, "Natural convection from rectangular interrupted fins," *Int. J. Therm. Sci.*, vol. 82, pp. 62–71, Aug. 2014. DOI: 10.1016/j.ijthermalsci.2014.03.016.

[17] D. Jeon and C. Byon, "Thermal performance of plate fin heat sinks with dual-height fins subject to natural convection," *Int. J. Heat Mass Transf.*, vol. 113, pp. 1086–1092, Oct. 2017. DOI: 10.1016/j.ijheatmasstransfer.2017.06.031.

[18] O. Sigmund and K. Maute, "Topology optimization approaches," *Struct. Multidisc. Optim.*, vol. 48, no. 6, pp. 1031–1055, 2013. DOI: 10.1007/s00158-013-0978-6.

[19] T. Dbouk, "A review about the engineering design of optimal heat transfer systems using topology optimization," *Appl. Therm. Eng.*, vol. 112, pp. 841–854, Feb. 2017. DOI: 10.1016/j.applthermaleng.2016.10.134.

[20] M. P. Bendsoe and O. Sigmund, *Topology Optimization: Theory, Methods, and Applications*, 2nd ed. Berlin, Germany: Springer, 2004.

[21] H. L. Li and B. Y. Cao, "Topology optimization of the volume-to-point heat conduction problem at micro- and nano-scale," *Acta Phys. Sin.-Ch. Ed.*, vol. 68, no. 20, pp. 10, 2019. DOI: 10.7498/aps.68.20190923.

[22] J. Alexandersen and C. Andreasen, "A review of topology optimisation for fluid-based problems," *Fluids*, vol. 5, no. 1, pp. 29, 2020. DOI: 10.3390/fluids5010029.

[23] L. Yin and G. K. Ananthasuresh, "A novel topology design scheme for the multi-physics problems of electro-thermally actuated compliant micro-mechanisms," *Sensor. Actuat. A-Phys*, vol. 97–98, pp. 599–609, Apr. 2002. DOI: https://doi.org/10.1016/S0924-4247. (01)00853-6. DOI: 10.1016/S0924-4247(01)00853-6.

[24] T. E. Bruns, "Topology optimization of convection-dominated, steady-state heat transfer problems," *Int. J. Heat Mass Transf*, vol. 50, no. 15–16, pp. 2859–2873, 2007. DOI: 10.1016/j.ijheatmasstransfer.2007.01.039.

[25] A. Iga, S. Nishiwaki, K. Izui and M. Yoshimura, "Topology optimization for thermal conductors considering design-dependent effects, including heat conduction and convection," *Int. J. Heat Mass Transf*, vol. 52, no. 11–12, pp. 2721–2732, 2009. DOI: 10.1016/j.ijheatmasstransfer.2008.12.013.

[26] E. M. Dede, S. N. Joshi and F. Zhou, "Topology optimization, additive layer manufacturing, and experimental testing of an air-cooled heat sink," *J. Mech. Design*, vol. 137, no. 11, pp. 9, Oct. 2015. DOI: 10.1115/1.4030989.

[27] M. Zhou, J. Alexandersen, O. Sigmund and C. B. W. Pedersen, "Industrial application of topology optimization for combined conductive and convective heat transfer problems," *Struct. Multidisc Optim.*, vol. 54, no. 4, pp. 1045–1060, 2016. DOI: 10.1007/s00158-016-1433-2.

[28] P. Coffin and K. Maute, "Level set topology optimization of cooling and heating devices using a simplified convection model," *Struct. Multidisc Optim.*, vol. 53, no. 5, pp. 985–1003, 2016. DOI: 10.1007/s00158-015-1343-8.

[29] J. Alexandersen, N. Aage, C. S. Andreasen and O. Sigmund, "Topology optimisation for natural convection problems," *Int. J. Numer. Meth. Fluids*, vol. 76, no. 10, pp. 699–721, 2014. DOI: 10.1002/fld.3954.

[30] P. Coffin and K. Maute, "A level-set method for steady-state and transient natural convection problems," *Struct Multidisc Optim*, vol. 53, no. 5, pp. 1047–1067, 2016. DOI: 10.1007/s00158-015-1377-y.

[31] J. Alexandersen, O. Sigmund and N. Aage, "Large scale three-dimensional topology optimisation of heat sinks cooled by natural convection," *Int. J. Heat Mass Transf*, vol. 100, pp. 876–891, Sep. 2016. DOI: 10.1016/j.ijheatmasstransfer.2016.05.013.

[32] J. Asmussen, J. Alexandersen, O. Sigmund and C. S. Andreasen, "A "poor man's" approach to topology optimization of natural convection problems," *Struct Multidisc Optim.*, vol. 59, no. 4, pp. 1105–1124, 2019. DOI: 10.1007/s00158-019-02215-9.

[33] N. Pollini, O. Sigmund, C. S. Andreasen and J. Alexandersen, "A "poor man's" approach for high-resolution three-dimensional topology design for natural convection problems," *Adv. Eng. Softw*, vol. 140, pp. 102736, Feb. 2020. DOI: 10.1016/j.advengsoft.2019.102736.

[34] J. Alexandersen, O. Sigmund, K. E. Meyer and B. S. Lazarov, "Design of passive coolers for light-emitting diode lamps using topology optimisation," *Int. J. Heat Mass Transf*, vol. 122, pp. 138–149, Jul. 2018. DOI: 10.1016/j.ijheatmasstransfer.2018.01.103.

[35] T. Lei, et al., "Investment casting and experimental testing of heat sinks designed by topology optimization," *Int. J. Heat Mass Transf*, vol. 127, pp. 396–412, Dec. 2018. DOI: 10.1016/j.ijheatmasstransfer.2018.07.060.

[36] B. S. Lazarov, O. Sigmund, K. E. Meyer and J. Alexandersen, "Experimental validation of additively manufactured optimized shapes for passive cooling," *Appl. Energ*, vol. 226, pp. 330–339, Sep. 2018. DOI: 10.1016/j.apenergy.2018.05.106.

[37] T. Borrvall and J. Petersson, "Topology optimization of fluids in Stokes flow," *Int. J. Numer. Meth. Fluids*, vol. 41, no. 1, pp. 77–107, 2003. DOI: 10.1002/d.426.

[38] L. H. Olesen, F. Okkels and H. Bruus, "A high-level programming-language implementation of topology optimization applied to steady-state Navier–Stokes flow," *Int. J. Numer. Meth. Engng*, vol. 65, no. 7, pp. 975–1001, 2006. DOI: 10.1002/nme.1468.

[39] H. Kaydani and A. Mohebbi, "Computational fluid dynamics simulation of two-dimensional natural convection in a fractured porous medium," *Heat Transfer Eng*, vol. 38, no. 18, pp. 1606–1615, 2017. DOI: 10.1080/01457632.2016.1255040.

[40] M. P. Bendsøe and O. Sigmund, *Optimization of Structural Topology, Shape, and Material*. Berlin, Germany: Springer, 1995.

[41] J. H. Klaas Haertel, K. Engelbrecht, B. S. Lazarov, and O. Sigmund, "Topology Optimization of Thermal Heat Sinks," in *COMSOL Conference 2015*, Grenoble, Switzerland, 2015.

[42] O. Sigmund and J. Petersson, "Numerical instabilities in topology optimization: A survey on procedures dealing with checkerboards, mesh-dependencies and local minima," *Struct. Optimization*, vol. 16, no. 1, pp. 68–75, 1998. DOI: 10.1007/BF01214002.

[43] B. S. Lazarov and O. Sigmund, "Filters in topology optimization based on Helmholtz-type differential equations," *Int. J. Numer. Meth. Engng*, vol. 86, no. 6, pp. 765–781, 2011. DOI: 10.1002/nme.3072.

[44] J. K. Guest, J. H. Prévost and T. Belytschko, "Achieving minimum length scale in topology optimization using nodal design variables and projection functions," *Int. J. Numer. Meth. Engng*, vol. 61, no. 2, pp. 238–254, 2004. DOI: 10.1002/nme.1064.

[45] F. Wang, B. S. Lazarov and O. Sigmund, "On projection methods, convergence and robust formulations in topology optimization," *Struct Multidisc Optim*, vol. 43, no. 6, pp. 767–784, 2011. DOI: 10.1007/s00158-010-0602-y.

[46] S. L. Xu, Y. W. Cai and G. D. Cheng, "Volume preserving nonlinear density filter based on heaviside functions," *Struct Multidisc Optim*, vol. 41, no. 4, pp. 495–505, 2010. DOI: 10.1007/s00158-009-0452-7.

[47] K. Svanberg, "The method of moving asymptotes - a new method for structural optimization," *Int. J. Numer. Meth. Engng*, vol. 24, no. 2, pp. 359–373, 1987. DOI: 10.1002/nme.1620240207.

[48] Y. A. Cengel and A. J. Ghajar, *Heat and Mass Transfer - Fundamentals and Applications*, 6th ed., New York, NY: McGraw-Hill Education, 2020.

[49] J. Dirker and J. P. Meyer, "Topology optimization for an internal heat-conduction cooling scheme in a square domain for high heat flux applications," *J. Heat Trans*, vol. 135, no. 11, pp. 10, Sep. 2013. DOI: 10.1115/1.4024615.